Mechanism and control of the metal-to-insulator transition in rocksalt tantalum nitride

L. Yu,[1] C. Stampfl,[2] D. Marshall,[3] T. Eshrich,[3] V. Narayanan,[1] J. M. Rowell,[1,4] N. Newman,[1,*] and A. J. Freeman[2]

[1]*Chemical and Materials Engineering Department and Electrical Engineering Department, Arizona State University,*
Tempe, Arizona 85287

[2]*Department of Physics and Astronomy, Northwestern University, Evanston, Illinois 60208-3112*

[3]*Motorola, Physical Sciences Research Labs, 7700 S. River Parkway, Tempe, Arizona 85284*

[4]*Materials Research Institute, Northwestern University, Evanston, Illinois 60208-3112*

We identify the previously unknown mechanism whereby rocksalt Ta_xN can be continuously tuned from conducting to insulating through changes in stoichiometry. Experimental measurements on thin films, combined with electronic structure calculations on a host of native defects, show that the tunability arises from changes in the free electron concentration as a result of localization at Ta vacancies (V_{Ta}). The observed enhanced resistivity, transition from electron to hole conduction at $x \sim 0.6$, and diminished mid-IR reflectance are consistent with the dominance of the V_{Ta} defect in nitrogen-rich material.

The metal-insulator transition occurs in doped semiconductors, quenched condensed metal films, metal-insulator mixtures, and inversion layers of field-effect transistors.[1,2] The physical properties of Ta_xN in the rocksalt structure are also found to span the range characteristic of this transition. While the widely varying properties have been recognized to some degree, the microscopic origin of this behavior is hitherto unknown. Ta_xN in the rocksalt structure is of considerable current interest and is used in, and has potential for, a wide range of technological applications. For example, Ta_xN is used as a diffusion barrier in copper interconnects on Si chips[3] and to make compact thin-film resistors. It exhibits superconductivity below 10 K (Refs. 4 and 5) and has been shown to hold promise as a barrier material in NbN-based Josephson junction 100+ GHz digital circuits when grown with a resistivity near the metal-insulator transition.[6]

In this paper, we characterize the chemical, electrical, optical, structural, and thermoelectric properties of Ta_xN films whose electrical properties are tuned from conducting to insulating by adjusting the stoichiometry. Theoretically, we investigate the electronic structure and formation energies of native point defects, focusing on the N-rich structures that have dramatically increased resistivities and are used in Josephson junction barrier layers. We also perform calculations for the nitrogen-rich, thermodynamically stable phases: namely, rocksalt Ta_4N_5 ($Ta_{0.8}N$) and orthorhombic Ta_3N_5 ($Ta_{0.6}N$).[7–9] Our results point conclusively to the V_{Ta} as being predominantly responsible for the metal-insulator transition in rocksalt Ta_xN. Vacancies in other nonstoichiometric transition-metal nitrides have been previously studied.[10] We extended this to the Ta_xN system.

Experimentally, Ta_xN is synthesized in a high-vacuum sputtering system equipped with a dc magnetron sputter gun (model Torus 2C, Kurt Lesker Co.) containing a 99.5%-pure 5.1-cm-diam Ta target. Two types of substrates are used: 1 cm^2 (0001) sapphire and 10.2-cm-diam (100) Si wafers coated with a 140-nm thermal SiO_2 layer. The sheet resistance is measured with a four-point probe. Hall measurements are made in the Van der Pauw configuration with a 1-T magnet. X-ray diffraction measurements are performed using

a Rigaku (model DMAX-A) diffractometer. Seebeck measurements are performed on a custom system with a stage containing a temperature gradient and two Chromel-Alumel thermocouples. The thermovoltage is measured between the two points, Chromel to Chromel and Alumel to Alumel, with this value applied to correct the thermocouple wire thermovoltage. Rutherford backscattering spectroscopy (RBS) is used to determine the chemical composition and film thickness. Optical reflectivity is measured using a Bruker infrared spectrometer (model IFS 86 w/s). High-resolution cross-sectional transmission electron microscopy (TEM) is performed on a Jeol microscope (model JEM-4000EX) operating at 400 keV with an interpretable resolution of 0.17 nm.

Density-functional-theory (DFT) calculations are performed using the first-principles full-potential linearized augmented plane wave (FLAPW) method[11] within the local-density approximation (LDA) with the Hedin-Lundqvist exchange-correlation functional.[12] We treat the core states fully relativistically and the valence states scalar-relativistically, and use angular momenta up to $l = 8$ in the muffin-tin spheres for both the wave functions and charge density in the self-consistent cycles. We consider high and low defect concentrations by creating the defects in ideal 8- and 32-atom TaN cells which model the defect systems in rocksalt Ta_xN. For the former, the energy cutoff for the plane-wave expansion in the interstitial region between the muffin-tin spheres is taken to be 25 Ry and also for the 18-atom $Ta_{0.8}N$ compound. For the larger "32-atom" systems (which includes the $Ta_{0.6}N$ structure), a slightly lower cutoff of 20.7 Ry was used. The atomic positions of all atoms are fully relaxed until the force on each atom is less than 1 mRy/a.u. Further calculation details can be found in Ref. 13.

Density functional calculations performed using the "8-atom" cell (high-concentration defect structures) for the N-vacancy (V_N), Ta-vacancy (V_{Ta}), N-antisite (N_{Ta}), and N-interstitial (N_i) induce a change in the equilibrium volume of -0.85%, -2.55%, -1.52%, and $+3.15\%$, respectively, when compared to stoichiometric defect-free TaN. Low-concentration "32-atom" defect systems are calculated using the theoretical stoichiometric TaN lattice constant of 0.437
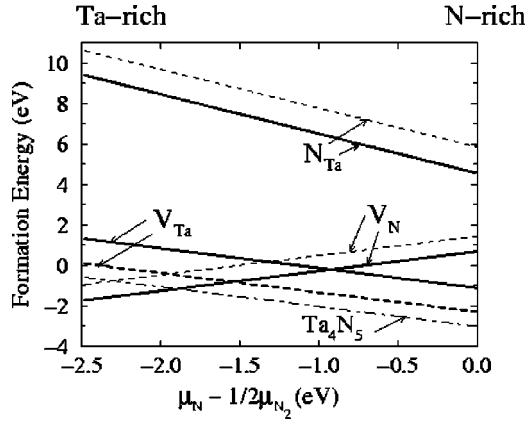
FIG. 1. Formation energies for native point defects in TaN; solid and dashed lines correspond to high and low defect concentrations, respectively, for the N-antisite (N_{Ta}), the N-vacancy (V_N), and the Ta-vacancy (V_{Ta}). The dot-dashed curve is the V_{Ta} formation energy (per vacancy) for the $Ta_{0.8}N$ compound found in nature.

FIG. 2. (a) Density of states (DOS) for bulk TaN, (b) the low-concentration V_{Ta} (calculated in the "32-atom" cell), (c) the high-concentration V_{Ta} (calculated in the "8-atom" cell), (d) an even higher-concentration V_{Ta} (calculated in a cell containing 10 N atoms and 6 Ta atoms), and (e) the $Ta_{0.8}N$ and (f) $Ta_{0.6}N$ compounds which form in nature. Total DOS (upper curves), total N and Ta partial DOS (lower curves), as indicated by the labels. N′ and N correspond to the partial DOS at the N atom away from and neighboring the Ta vacancy, respectively.

nm (the experimental value is 0.4385 nm).[7–9] The six nearest-neighbor atoms to the V_{Ta}, V_N, and N_{Ta} sites relax inwards by 3%, 7%–10%, and 8%–10%, respectively, in the fully relaxed geometry. The equilibrium volume of the thermodynamically stable structure, $Ta_{0.8}N$, is calculated to be 1.81% smaller than the corresponding theoretical stoichiometric TaN volume and is 1.2% smaller than the experimental value. We also fully relaxed the internal coordinates and find very good agreement with experiment.[7–9] For the larger and more complex $Ta_{0.6}N$ structure, we only optimized the equilibrium volume where it is 0.1% smaller than experiment.

We calculate the formation energy as $E_f = E_{tot}^{defect} - n E_{tot}^{bulk} + n_{Ta}\mu_{Ta} + n_N\mu_N$, where E_{tot}^{defect} and E_{tot}^{bulk} are the total energies of the defect calculated using the supercell and a bulk TaN unit, respectively, and n is the number of Ta (and N) atoms in the ideal supercell (i.e., without a defect). n_{Ta} and n_N are the number of Ta and N atoms, and μ_{Ta} and μ_N are the corresponding chemical potentials, which account for atoms that are added to, or taken from, the ideal supercell to create the defect under consideration. We assume both species are in thermal equilibrium with bulk TaN; thus, $\mu_{Ta} + \mu_N = \mu_{TaN}$ where μ_{TaN} is the chemical potential of TaN. We also have the boundary conditions $\mu_N < 1/2\mu_{N_2}$ and $\mu_{Ta} < \mu_{Ta(bulk)}$, where μ_{N_2} and $\mu_{Ta(bulk)}$ are the chemical potentials of (two) N atoms in the nitrogen molecule and of a Ta atom in bulk Ta, respectively. For nitrogen-rich conditions, we set $\mu_N = 1/2\mu_{N_2}$ and for tantalum-rich conditions, we set $\mu_{Ta} = \mu_{Ta(bulk)}$. With these constraints, the range of the nitrogen chemical potential is $-\Delta H_f^0 < \mu_N - 1/2\mu_{N_2} < 0$, where the heat of formation is $\Delta H_f^0 = \mu_{Ta(bulk)} + 1/2\mu_{N_2} - \mu_{TaN}$. Calculations of bulk Ta and TaN and the N_2 dimer are also required and details of these are reported in Ref. 13 in which the calculated heat of formation is -2.48 eV. The calculated formation energies as a function of the nitrogen chemical potential are shown in Fig. 1.
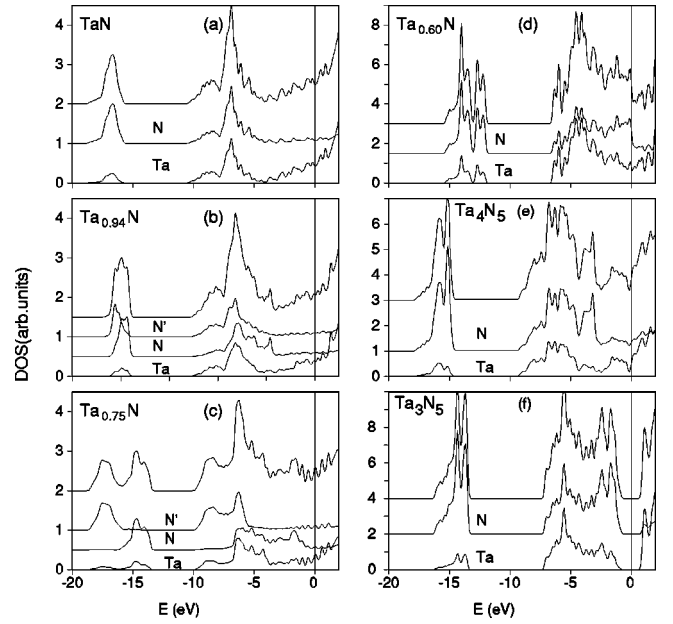
The calculations indicate that V_{Ta} and V_N have by far the lowest formation energies for N- and Ta-rich conditions, respectively. The dominance of vacancies in nonstoichiometric Ta_xN is consistent with the conclusions of a recent x-ray emission study.[14] Later in this paper, we will show that the electrical, optical, and thermoelectric properties of nitrogen-rich Ta_xN can be attributed to the dominance of the V_{Ta} defect. The N_i is energetically very unfavorable (not shown in Fig. 1; values range from ~14.9 to 12.4 eV for Ta- and N-rich conditions, respectively) and the next most unfavorable is the antisite (or substitutional) defect N_{Ta}. The V_N formation energy is lower for the higher concentration, and for the V_{Ta} it is the opposite. The V_{Ta} in the ordered rocksalt $Ta_{0.8}N$ compound has the lowest energy, consistent with the fact that it forms in nature.

Figures 2(a), 2(b), and 2(c) show total and partial density of states for stoichiometric TaN, the low-concentration V_{Ta} (calculated in the "32-atom" cell), and the high-concentration V_{Ta} (calculated in the "8-atom" cell), respectively. Also shown in Fig. 2(d) is an even higher-concentration V_{Ta} system corresponding to a defective rocksalt structure ($Ta_{0.6}N$) as calculated in a cell containing 10 N atoms and 6 Ta atoms. The V_N and the N_{Ta} (not shown) have a relative DOS at E_F similar to, or higher than, stoichiometric TaN, i.e., similar to a conventional metal. These defects act "donorlike" in that they add free electrons to the conduction band. In contrast, the Ta-vacancy structures have a *reduced* DOS at E_F as compared to bulk TaN. In particular,
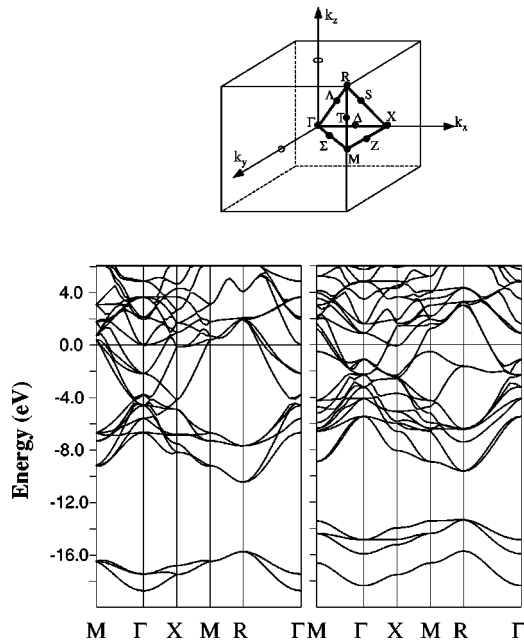
FIG. 3. Band structure of bulk rocksalt TaN as calculated in an 8-atom cell (left) and, right, that of the Ta-vacancy structure [corresponding to the DOS in Fig. 2(c)]. Also shown is the corresponding Brillouin zone and high-symmetry lines and points.

it can be seen that with increasing V_{Ta} concentration, the DOS at E_F diminishes monotonically, with a corresponding reduction in the free carrier concentration. V_{Ta} is therefore "acceptorlike" in that it spatially localizes free carriers in the conduction band. For V_{Ta}, an increase in the number of states in the region -1 to -4 eV below E_F can also be seen [Fig. 2(c)]. For the "low-concentration" case, only a sharp feature around -4 eV below E_F occurs [Fig. 2(b)]. Inspection of the band structure shows that the latter features are defect-related states. Also, the $2s$-like state of the neighboring N atom is at a higher energy than in stoichiometric TaN, as would be expected from charge transfer to an acceptor site.

Figure 3 (right) shows the band structure for the V_{Ta}, corresponding to Fig. 2(c), where the Brillouin zone and high-symmetry lines and points are illustrated. For comparison, the ideal stoichiometric TaN bulk band structure is shown (left), as calculated also using the "8-atom" cell. From Fig. 3 (right), it can be seen that a defect-related state occurs around -17 eV, as well as in the energy range -1 to -4 eV (seen most clearly around the M-R-Γ region).

Figures 2(e) and 2(f) show the total and partial density of states for two phases that form in nature: $Ta_{0.8}N$, an ordered defect configuration in the rocksalt structure, and $Ta_{0.6}N$, an orthorhombic structure. For $Ta_{0.8}N$, the DOS at E_F exhibits a sharp minimum, in contrast to stoichiometric TaN. New features at around -3 to -5 eV below E_F also occur. There is an upward shift in the N-$2s$ level, as seen for other tantalum-vacancy systems. In contrast to the very small, but finite, DOS at E_F for rocksalt $Ta_{0.6}N$ [Fig. 2(d)], the orthorhombic $Ta_{0.6}N$ structure exhibits a 1.5 eV band gap [Fig. 2(f)]. The insulating nature can be understood from electron counting
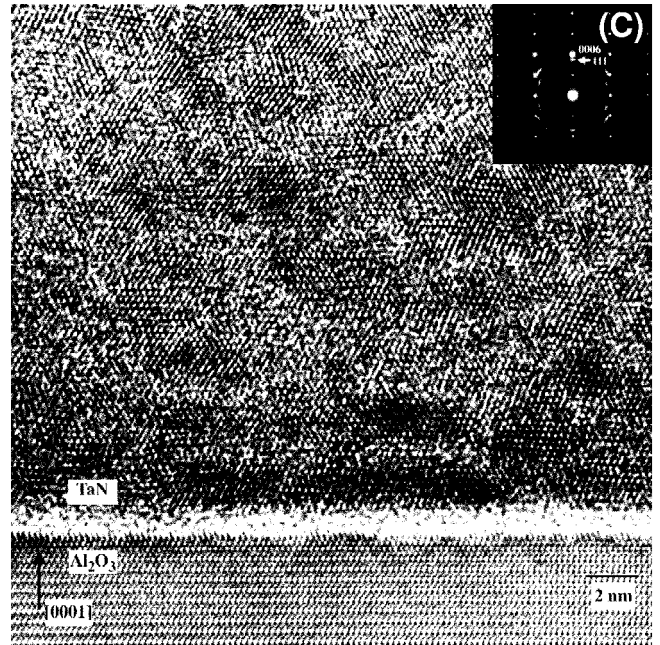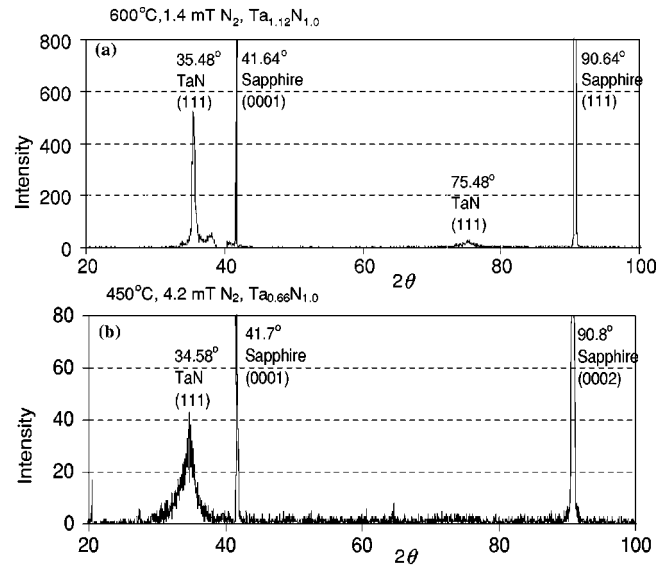

FIG. 4. X-ray diffraction data of (a) near-stoichiometric and (b) nitrogen-rich Ta_xN, respectively. The near-stoichiometric film has a composition of $Ta_{1.12}N$ and was grown at 600 °C in 1.4 mT nitrogen partial pressure. The nitrogen-rich film has a composition of $Ta_{0.66}N$ and was grown at 450 °C in 4.2 mT nitrogen partial pressure. (c) Cross-sectional TEM image and selected-area diffraction pattern (inset) of a nitrogen-rich $Ta_{0.66}N$ film grown at 450 °C in 4.2 mT nitrogen partial pressure. The material has a ~ 5 nm subgrain mosaic structure with misorientations on the order of $\pm 5°$ (as most easily seen in the diffraction pattern). The predominant in-plane epitaxial orientations are $TaN(111)\|Al_2O_3$ (001) and $TaN(1\bar{1}10)\|Al_2O_3$ ($1\bar{1}00$).

since there are 40 valence electrons (3×5 from Ta plus 5×5 from N) and the s and p bands of the five nitrogen atoms can accommodate exactly $5\times 8=40$ electrons.

X-ray diffraction and TEM measurements indicate that films synthesized in this study are comprised of rocksalt Ta_xN oriented in the $\langle 111 \rangle$ growth direction. Metallic Ta_xN
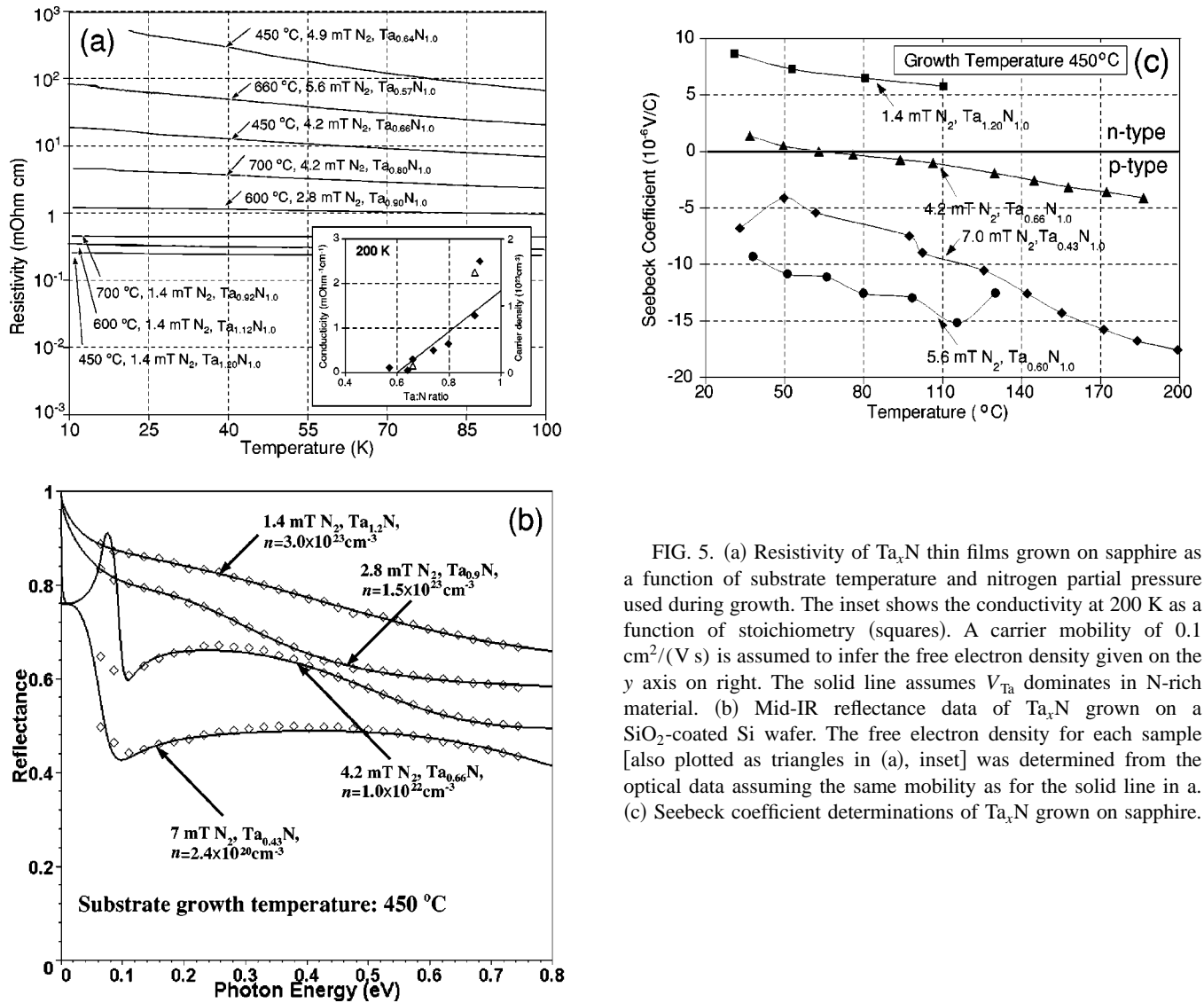
FIG. 5. (a) Resistivity of Ta$_x$N thin films grown on sapphire as a function of substrate temperature and nitrogen partial pressure used during growth. The inset shows the conductivity at 200 K as a function of stoichiometry (squares). A carrier mobility of 0.1 cm^2/(V s) is assumed to infer the free electron density given on the y axis on right. The solid line assumes V_{Ta} dominates in N-rich material. (b) Mid-IR reflectance data of Ta$_x$N grown on a SiO$_2$-coated Si wafer. The free electron density for each sample [also plotted as triangles in (a), inset] was determined from the optical data assuming the same mobility as for the solid line in a. (c) Seebeck coefficient determinations of Ta$_x$N grown on sapphire.

films produced at reduced nitrogen pressures ($<$1.4 mTorr nitrogen partial pressure) are crystalline with a near-bulk lattice constant of 0.439 nm, as evidenced by the dominance of the (111) x-ray diffraction Bragg peak at 35.5° with a full width at half maximum (FWHM) of 0.5° [Fig. 4(a)]. For films with a N:Ta ratio greater than 1.5, a much wider Bragg peak at $\sim$34.6° with a FWHM of 2.6° is found [Fig. 4(b)]. The extended lattice constant ($\sim$0.450 nm) and wide diffraction peaks are typical of oriented nanocrystalline material as a result of the significant fraction of material in the grain boundary regions under tensile stress.[15] This conclusion is consistent with TEM results. Figure 4(c) illustrates a cross-sectional TEM image of a nitrogen-rich film grown under the same deposition conditions used to produce barrier layers in Josephson junctions exhibiting large characteristic voltages ($>$2 mV). The material has a $\sim$5-nm subgrain mosaic structure with misorientations on the order of $\pm$5°. Figure 5(a) shows that there is a clear trend between the increase in N content in the films, enhancement in resistivity, ρ, and reduction in resistivity ratio, ρ(300 K)/ρ(20 K). The conductivity at 200 K in the same samples as in Fig. 5(a) is

plotted as a function of stoichiometry in the inset. The conductivity follows a monotonic drop from a large metallic value for stoichiometric TaN, to a minimum value near Ta$_{0.6}$N. The trend line was derived assuming a constant electron mobility [0.1 cm^2/(V s)] and a free electron density resulting from the contribution of two electrons per occupied TaN pair in conjunction with a reduction of five free electrons per pentavalent V_{Ta} acceptor. Note that the experimental values fall near this trend line. The observed minimum at a Ta:N ratio of 0.6 is strong evidence for the dominance of the pentavalent V_{Ta} acceptor in the nitrogen-rich material. Hall measurements are only able to give an upper bound of 0.1 cm^2/(V s) at room temperature due to the limited resolution possible when measuring low-mobility samples with a low-field magnet, but are consistent with the value derived from the trend line.

Mott[1] proposed that the metal-insulator (M-I) transition occurs at a resistivity of $Kh\alpha/q^2$ where K is a constant between $\sim$3 and 6, h is Planck's constant, q is the electron charge, and α is a characteristic length corresponding to a value on the order of the Bohr radius for Mott insulators and

the mean free path for Anderson insulators. From the measured upper bound of mobility in our samples, a mean free path of 0.05 nm is inferred. Although this corresponds to an unphysically small value, we expect that α will fall between this value and the bond distance (0.22 nm), resulting in a M-I transition between ~ 0.4 and 4 mΩ cm from Mott's analysis.

In Fig. 5(b) we show the mid-infrared (MIR) reflectance of Ta$_x$N. The decreased reflectance in films with increasing nitrogen content is attributed to the reduction of free carriers. To infer the free carrier concentration from the optical data, a mean least-squares fit was performed assuming the same mobility used to determine the trendline in Fig. 5(a), inset, and standard equations for the dielectric function and the reflectance of a Drude free electron gas in the presence of a single-phonon model.[16] It is clear that the free carrier densities determined from the electrical and optical data are similar when a common value for mobility is used.[17]

In Fig. 5(c), the Seebeck coefficient of sputtered Ta$_x$N thin films is illustrated. Films with Ta:N ratios less than ~ 0.66 have predominantly hole (p-type) conduction. The drop in the Seebeck coefficient for Ta$_{0.43}$N is not unexpected since this sample also exhibits a decreased electrical resistivity [not shown in Fig. 5(a)], presumably as a result of enhanced hole doping. We note that from thermoelectric data alone, it is difficult to give a quantitative estimate of the number of charge carriers since the Seebeck coefficient is a strong function of electron conductivity, density of states, and carrier type. This transition from hole to electron domi-nant thermovoltage occurs at a stoichiometry of Ta$_{0.66}$N, which is slightly lower than expected (i.e., Ta$_{0.6}$N). For these films, the inhomogeneous nature of the material, as well as the large number of defects present, will influence the number and type of free carriers in the films. Anderson localization would also be expected to drive the material insulating at lower nitrogen content than for ordered material, as is observed experimentally. It is clear that the observed properties are strong evidence for the dominance of the V_{Ta} defect and are inconsistent with the dominance of the other nitrogen-rich defects, including the N$_{Ta}$ defect.

In summary, the electrical properties of rocksalt Ta$_x$N can be finely tuned from highly conductive to insulating through adjustment of stoichiometry. The dominance of the V_{Ta} under N-rich conditions is predicted theoretically and is consistent with the experimentally observed electrical, optical, and thermal properties.

---

*Corresponding author.

[1] N. Mott, Proc. R. Soc. London, Ser. A **382**, 1 (1982) and references therein.

[2] R. C. Dynes and P. A. Lee, Science **223**, 355 (1984); G. A. Thomas, A. Kawabata, Y. Ootuka, S. Katsumoto, S. Kobayashi, and W. Sasaki, Phys. Rev. B **26**, 2113 (1982); G. Timp, A. B. Fowler, A. Hartstein, and P. N. Butcher, *ibid.* **34**, 8771 (1986) and references therein.

[3] M. H. Tsai, S. C. Sun, C. P. Lee, H. T. Chiu, C. E. Tsai, S. H. Chuang, and S. C. Wu, Thin Solid Films **270**, 531 (1995).

[4] K. Wakasugi, M. Tokunaga, T. Sumita, H. Kubota, M. Nagata, and Y. Honda, Physica B **239**, 29 (1997).

[5] K. Reichelt, W. Nellen, and G. Mair, J. Appl. Phys. **49**, 5284 (1987).

[6] A. B. Kaul, L. Yu, N. Newman, J. M. Rowell, S. R. Whiteley, and T. Van Duzer, Appl. Phys. Lett. **78**, 99 (2001); T. van Duzer, L. Zheng, X. Meng, C. Loyo, S. R. Whiteley, L. Yu, N. Newman, J. M. Rowell, and N. Yoshikawa, *Superconductivity and its Applications* [Physica C (to be published)].

[7] R. W. G. Wyckoff, *Crystal Structures*, 2nd ed. (Wiley, New York, 1982), Vol. 1, p. 86.

[8] *Structure Reports*, edited by W. B. Pearson (International Union of Crystallography, Oosthoek, Scheltema, and Holkema, Utrecht, 1976), Vol. 35A, p. 121.

[9] N. E. Brese, M. O'Keeffe, P. Rauch, and F. J. DiSalvo, Acta Crystallogr., Sect. C **47**, 2291 (1991).

[10] See, for example, V. Gubanov and A. Ivanovsky, *Density Functional Theory of Molecules, Clusters, and Solids* (Kluwer Academic, Dordrecht, 1995), pp. 223–261; P. Blaha, J. Redinger, and K. Schwarz, Phys. Rev. B **31**, 2316 (1985) and references therein.

[11] E. Wimmer, H. Krakauer, M. Weinert, and A. J. Freeman, Phys. Rev. B **24**, 864 (1981).

[12] L. Hedin and B. I. Lundqvist, J. Phys. C **4**, 2064 (1971).

[13] C. Stampfl, W. Mannstadt, R. Asahi, and A. J. Freeman, Phys. Rev. B **63**, 155 106 (2001); and (unpublished).

[14] O. Yu. Khyzhun and Y. V. Zaulchny, Phys. Status Solidi B **207**, 191 (1998).

[15] H. Gleiter, Prog. Mater. Sci. **33**, 223 (1989).

[16] S. Pekowitz, *Optical Characterization of Semiconductors* (Academic, London, 1993), pp. 11–12, 39–40.

[17] Since a constant product of the free carrier density and mobility results in similar fits, we must be cautious in using these results to validate our conclusions. Nevertheless, the values derived are physically reasonable and subject to further investigation.